Article

Wetting of Refractory Ceramics with High-Manganese and Structural Steel and Description of Interfacial Interaction

Vlastimil Novák [1,*] , **Lenka Řeháčková** [1] , **Silvie Rosypalová** [1] **and Dalibor Matýsek** [2]

1   Faculty of Materials Science and Technology, VŠB-Technical University of Ostrava, 17. listopadu 15, Poruba, 708 00 Ostrava, Czech Republic
2   Faculty of Mining and Geology, VŠB-Technical University of Ostrava, 17. listopadu 15, Poruba, 708 00 Ostrava, Czech Republic
*   Correspondence: vlastimil.novak@vsb.cz

Abstract: This work aims to describe the interfacial interaction at the interface between refractory material and high-manganese (XT 720) and structural (11 523) steel using a wetting test up to 1600 °C. The contact angles were determined through the sessile drop method, and the results were put into context through degradation testing and the characterization of the interfacial interface by Energy Dispersive X-Ray (EDX), X-Ray Diffraction (XRD) analyses, and Scanning Electron Microscopy (SEM). The lowest resistance to molten steel was observed for chamotte materials, while the highest was observed for materials based on electrofused corundum. High-manganese steel was strongly erosive to the materials tested, with the wetting angle decreasing significantly from 10 to 103° with decreasing Al_2O_3 content (an increase of 2.4 to 59.4% corundum) in the refractories. Structural steel showed wetting angles from 103 to 127° for identical refractories. These results were consistent with the average erosion depth for Mn steel (0.2–7.8 mm) and structural steel (0–2.4 mm).

Keywords: high-manganese steel; structural steel; phase interface; reactive wetting; contact angle; refractory material

1. Introduction

High-alloy steels, such as manganese steel with the designation XT 720, are in high demand in technical practice, primarily because of their ability to harden when exposed to sufficiently strong impact loads and pressures. This gives the steel a high resistance to abrasive wear, making it suitable for the construction of excavators and other mining equipment. It is also widely applied in the national defense, automobile, and petrochemical industries due to its excellent strength, plasticity, and low-temperature flexibility [1,2]. However, some alloying elements contained in these steels have an adverse effect on refractory ceramics, whose participation in steel casting is essential. Refractories are necessary components not only in casting steels in the form of ingots but also in melting non-ferrous alloys. They serve as linings for thermal aggregates and furnaces and casting routes for transferring molten steel to the mold. They are also used to produce melting pots for the recovery of non-ferrous intermetallic alloys [3–5]. The steel and foundry industry is continuously focusing on developing and improving products, mainly in terms of their physical and mechanical properties. In this context, it is crucial to study the effect of refractory material on the steels with which it is in contact to maintain steel chemical composition within the required range, to achieve the desired cleanliness concerning the amount and character of non-metallic inclusions, and to prevent defects on the steel surface [6–8].

Chamotte and high-alumina materials are commonly used in the refractory industry to design casting routes. The latter are high-quality ceramic materials possessing high strength, heat resistance, low porosity, and high resistance to the erosive action of the melt. These properties are of great importance, as poor quality casting routes can cause the

release of unwanted elements into the melt due to ongoing reactions between the ceramic and the melt, which affects the purity of the steel and its microstructure, closely related to its final performance [9–11]. In secondary steel production, one of the main challenges is to ensure high steel cleanliness, which is influenced, among other things, by the resistance of the refractory material during the production process. In particular, non-metallic inclusions are a source of considerable concern as they can act as stress enhancers in cast steels. For this reason, one of the indicators of steel quality is the amount of non-metallic inclusions present [12–16].

One method of assessing the degree of interaction between molten steel and an arbitrary substrate is through a high-temperature wetting test [17]. Wettability is the ability of a liquid to spread on a substrate. It is measured as the contact angle between a tangent drawn at the triple point and the substrate surface [18]. The spreading of a liquid on a substrate without reaction/absorption of the liquid by the substrate material is termed non-reactive wetting, while a wetting process affected by a reaction between the spreading liquid and the substrate material is termed reactive wetting. In most publications, the equilibrium contact angle is given respecting Young's equation, which puts the interfacial tensions into relation. However, it should be noted that the latter was derived assuming the spreading of a non-reactive liquid on a physically and chemically inert, smooth, and homogeneous substrate [19,20]. The wetting of a solid by a liquid is a complex phenomenon depending on many factors. In the case of non-reactive wetting, it is controlled by the physical properties of the spreading liquid and wetting system, chemical heterogeneity causing wetting hysteresis, surface roughness, and gaseous environment [21]. Conversely, the reactive wetting process is influenced by several other factors such as the use of flux added to reduce the barrier effects of the oxide layers, the addition of trace impurities, etc. [19,22,23].

The interaction between refractories and manganese steel has been studied by several researchers [24–28]. Wang et al. investigated the interfacial reactions between high-Mn and Al steel, MgO-C refractory material, and $CaO-SiO_2-Al_2O_3-MgO$ refining slag concerning the effect of complex reactions on steel purity [24]. Alibeigi et al. investigated the reactive wetting of several steels containing manganese up to approximately 5 wt% during annealing, finding that the strength of the wetting in a given arrangement is a function of the partial pressure of oxygen and is directly related to the thickness of the outer MnO film formed and not to the Mn content of the alloy [25]. Articles on similar topics can be found elsewhere [26,27]. Kong et al. observed the formation of interfacial layers of (Mn, Mg)O and $(Mn, Mg)O·Al_2O_3$ as a result of the interaction between medium-manganese steel and the refractory material MgO [28].

The objective of this paper was to describe the interaction at the interface of high-manganese steel and structural steel with a refractory ceramic material through a wetting test and to find a relationship between wetting and the erosive action of the melt. The phase interface after high-temperature tests was also characterized by SEM, EDX, and XRD analyses. Knowledge of interfacial behavior improves an understanding of the processes and reactions occurring at the interphase at elevated temperatures. Based on such tests, it is possible to optimize refractory ceramics in terms of their composition or physicochemical properties, which is vital for enhancing the casting process's quality and minimizing the ceramic material's negative influence on the final product.

2. Materials and Methods

2.1. Specification and Preparation of Samples

Six types of refractory ceramic materials produced by SEEIF Ceramic a.s. were selected for the wetting tests, differing in their physicomechanical properties, chemical and mineralogical composition, firing temperature, application, and cost of the final product. A detailed characterization of the physical properties of the studied ceramic materials determined according to the standard EN 993-1:2018 (Methods of test for dense shaped

refractory products—Part 1: Determination of bulk density, apparent porosity and true porosity) is given in Table 1.

Table 1. Physical properties of ceramic materials.

Sample	Firing Temperature [°C]	Volumetric Weight [g·cm^{-3}]	Water Absorption [%]	Apparent Porosity [%]
F 36	1250	2.03	12.48	25.4
ZR 50	1280	2.97	6.29	18.7
B 70	1250	2.36	8.95	21.1
ML 65	1250	2.37	8.83	20.9
M 70	1380	2.45	8.83	21.6
MK 82	1380	2.61	8.75	22.9

A Bruker-AXS D8 powder X-ray diffractometer was used to determine the mineralogical composition of the refractory specimens (Table 2).

Table 2. Mineralogical composition of ceramic materials [wt%].

Sample	Corundum	Mullite	Cristobalite	Quartz	Zircon	Baddeleyite	Amorphous phase
F 36	2.4	45.6	0.9	6.9	—	—	44.2
ZR 50	14.4	26.4	—	—	54.1	5.1	—
B 70	23.7	35.1	3.2	4.0	—	—	34.0
ML 65	17.9	46.7	0.2	0.5	—	—	34.7
M 70	26.2	45.3	0.3	1.0	—	—	27.2
MK 82	59.4	24.4	—	0.1	—	—	16.1

The ceramic materials were prepared from pure components by accurately batching them into a wheel mixer according to process guidelines (SEEIF Ceramic, a.s.). The mixture was moistened with water (the water content was between 10 and 15 wt%) and thoroughly mixed to ensure homogeneity. The molding was carried out using a press operating at a specific pressure of up to 10 MPa. From the materials thus prepared, plates with dimensions of $25 \times 25 \times 5$ mm were made. The chemical composition of the prepared refractories is listed in Table 3.

Table 3. Chemical composition of ceramic materials [wt%].

Sample	Al_2O_3	SiO_2	TiO_2	Fe_2O_3	CaO	MgO	K_2O	Na_2O	ZrO_2
F 36	40.3	54.5	1.6	1.8	0.3	0.3	1.0	0.2	—
ZR 50	23.1	35.4	0.7	0.8	0.2	0.2	0.6	0.3	38.7
B 70	70.5	23.7	2.5	1.9	0.3	0.2	0.8	0.1	—
ML 65	64.1	30.8	1.7	1.7	0.4	0.2	0.9	0.2	—
M 70	72.6	25.2	0.5	0.6	0.1	0.1	0.7	0.2	—
MK 82	83.1	14.8	0.4	0.6	0.1	0.1	0.6	0.3	—

Contact angles (wetting angles) were determined at the steel/ceramic interface. Two steels were selected for the wetting tests, XT 720 high manganese abrasion resistant steel and 11 523 low alloy structural steel, whose chemical composition was obtained using a SPECTRUMA GDA-750 HP glow discharge optical emission spectrometer, while the content of oxygen, sulfur, and carbon was measured with an ELTRA 2000 ONH and 2000 CS combustion analyzer. The results of the analyses are presented in Table 4.

Cubes with an edge length of 4.5 mm were manufactured from these steels by electro-spark machining. Before the experiment, the surface of the metal samples was first cleaned mechanically and then cleaned with acetone to remove oxides. Likewise, the surface of the ceramic materials was cleaned with acetone immediately prior to the wetting test.

Table 4. Chemical composition of XT 720 and 11 523 steels [wt%].

Steel	C	Mn	Si	P	S	Cu	Ni	Cr	Mo	V	Ti	Al	N
XT 720	1.29	19.33	0.73	0.04	0.004	0.11	0.10	1.99	0.06	0.02	0.01	0.04	0.03
11 523	0.22	0.67	0.40	0.01	0.003	0.09	0.11	0.14	0.03	—	—	—	0.01
The remainder up to 100 wt% was iron.													

2.2. Determination of Wetting Angles

The wetting angles were determined according to the sessile drop method in a CLASIC high-temperature observation furnace within the temperature range from the melting point of the steel sample to 1600 °C (Figure 1). The prepared samples (steel/ceramic substrate) were placed in the furnace tube, which was then hermetically sealed, evacuated to 0.1 Pa, and purged with argon of high purity (>99.9999%). The last two steps were repeated. The temperature program consisted of a 2 °C·min^{-1} temperature ramp rate ending at a maximum temperature of 1600 °C. A Pt-13% Rh/Pt thermocouple, which was placed near the sample, registered the temperature. To prevent oxidation of the sample, all measurements were carried out in an inert atmosphere of argon. A CANON EOS 550D high-resolution camera took images of drop silhouettes during the heating ramp. The wetting angles were evaluated using the ADSA (axisymmetric drop shape analysis) method based on fitting the drop profiles to a Laplacian curve using a nonlinear regression procedure [29].
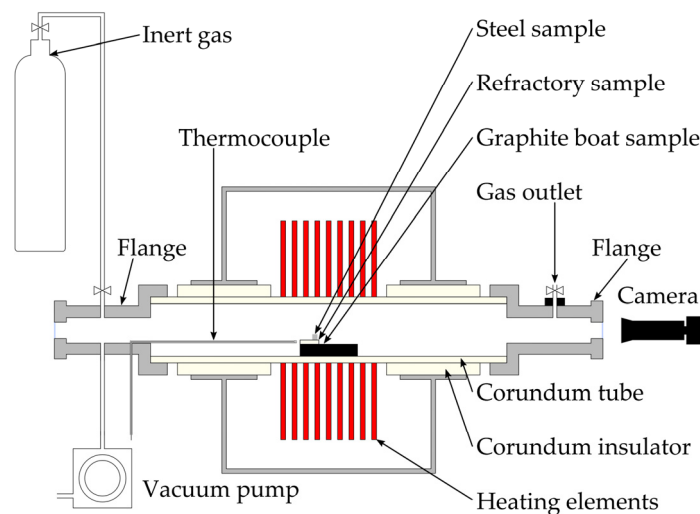
Figure 1. Schematic of the apparatus for the high-temperature wetting tests.

2.3. Degradation Testing of Refractory Materials

Degradation tests provide information on the resistance of the refractory material to molten steel. The tests were carried out in a TERMEL ITEP001 tilt induction furnace with a maximum power of 15 kW and a frequency range of 10–12 kHz. The furnace consists of a rectifier, a filtering capacity, an intermediate circuit, an inverter, a SIEMENS control system, and a cooling system. The maximum attainable temperature is 1700 °C. The steel melting was carried out in ceramic crucibles with dimensions of 125 × 85 × 45 mm made of the refractory materials under test. Cylinders with a diameter of 40 mm and a length of 68 mm were made from the steel specimens. The melting of the steel took 30 min, starting from the moment the steel was melted. During the melting process, the slag forming on the surface was removed. The temperature of the melt was measured with a thermocouple. After cooling, the crucible was cut along the central axis and prepared for evaluation of the ceramic's erosion losses due to the steel's action.

2.4. SEM, EDX, and XRD Methods

After the experiments, the interaction between the steel samples and ceramic crucibles was assessed by a JEOL 6490LV scanning electron microscope (SEM) equipped with an INCA EDX (Energy Dispersive X-ray Spectroscopy) analyzer enabling X-ray analysis of microsized particles and the determination of the chemical composition. The settings were as follows: thermos-emission cathode LaB6 and voltage 20 kV. The specimen chamber was kept at a high vacuum.

The phase composition of the ceramics crucibles after interaction with the steels was measured by a Bruker AXS D8 Advance X-ray diffractometer equipped with a LynxEye position-sensitive silicon strip detector under the following conditions: CuKα/Ni-filtered radiation, voltage 40 kV, current 40 mA, step mode with a step of 0.014$°$ 2θ, total time 25 s per step, and 2θ range 5–80$°$. The data were processed by Bruker AXS Diffrac and Bruker EVA software. The PDF-2 database (International Centre for Diffraction Data) was used for phase identification.

3. Results and Discussion

3.1. Wetting Tests

The temperature dependencies of the contact angles at the XT 720 steel/ceramic interface are shown in Figure 2.
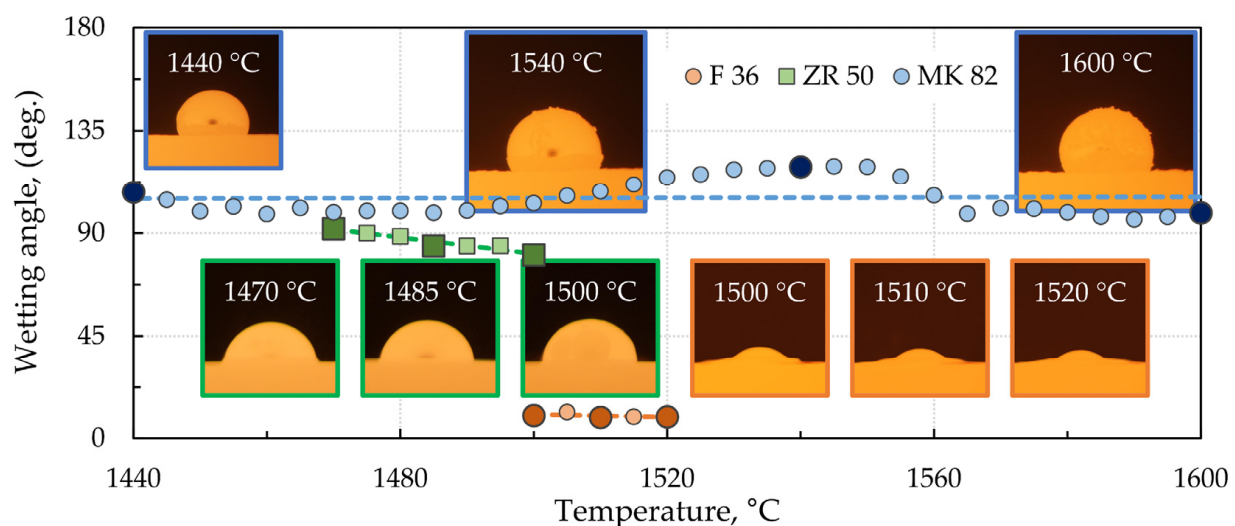

Figure 2. Temperature dependencies of the contact angles at the XT 720 steel/ceramic interface.

Since high-alloy manganese steel showed a severe interaction at the interface with the investigated ceramic material, only three temperature dependencies of the contact angles are selected in Figure 2, namely, with the basic fireclay material F36, the zirconia material ZR50, and the high corundum material MK82. The most pronounced interaction is observed at the interface with the material designated F36, with an apparent wetting angle of only about 10$°$ at temperatures around 1500 $°$C for this material with manganese steel. In the case of zirconia material ZR 50, the apparent wetting angle at the same temperature is 80$°$, and that of MK 82 is 103$°$. Though the temperature dependencies of the wetting angle were investigated up to a maximum temperature of 1600 $°$C, not all the angles could be adequately evaluated. Therefore, only the evaluable sections are shown in Figure 2, including images of the recorded droplets at the specified temperatures. A discussion regarding the interaction at these phase interfaces is given in Section 3.3.

Figure 3 shows the temperature dependencies of the wetting angles at the 11 523 steel/ceramic substrate interface. The low-alloy 11 523 structural steel showed considerably weaker interaction than the high-alloy Mn steel on the refractory surfaces investigated. The most significant interaction occurred at the interface with the conventional F 36 fireclay material.

In the temperature range of 1540–1600 °C, the contact angles ranged from 105° to 102°, while the lowest interaction was observed for the high corundum material MK82, where the contact angles in the same temperature range were 130°–123°. The values of the contact angles decrease slightly with increasing temperature as the sulfur content is less than 60 ppm [30,31].
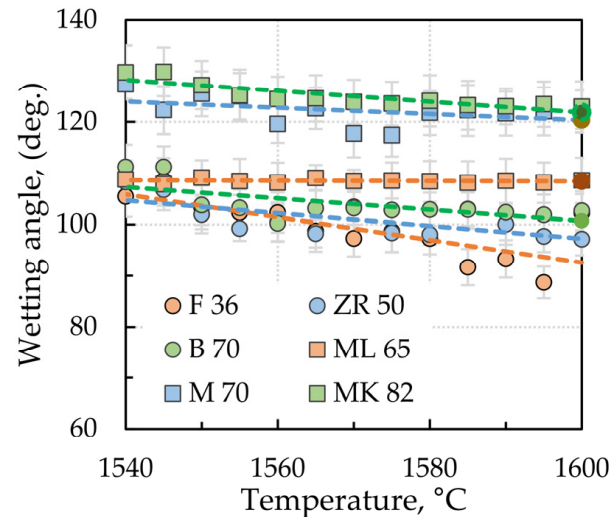

Figure 3. Temperature dependencies of contact angles at the 11 523 steel/ceramic interface (error lines parallel to the y-axis).

Images of the steel droplets observed on the ceramic material, including contact angle values at 1500 °C for XT 720 steel and at 1550 °C for 11 523 steel, are shown in Figures 4 and 5, respectively.
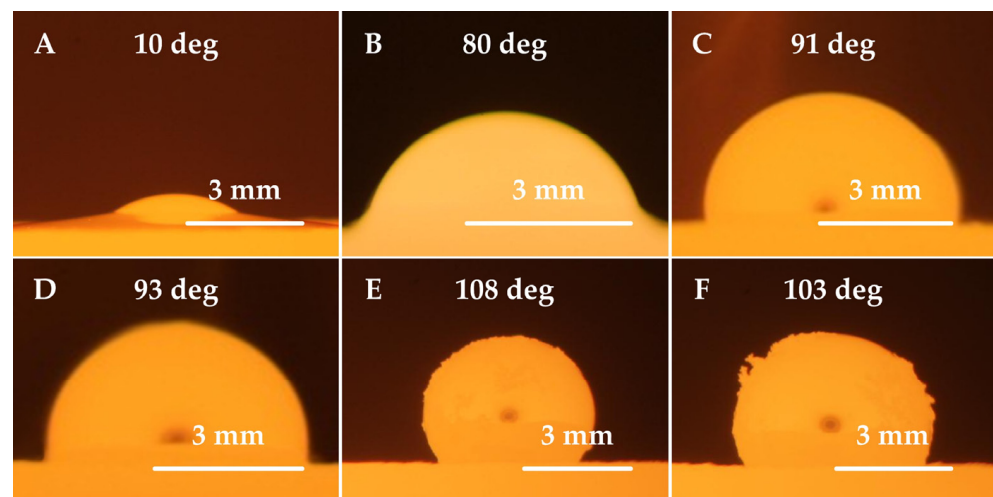

Figure 4. Images of XT 720 steel droplets wetting refractory ceramic substrates at 1500 °C; (**A**) F 36 ceramics, (**B**) ZR 50 ceramics, (**C**) B 70 ceramics, (**D**) ML 65 ceramics, (**E**) M 70 ceramics, and (**F**) MK 82 ceramics.

In general, when the wetting angle $\Theta \geq 90°$, the liquid (melt) exhibits non-wetting behavior towards the substrate. If the wetting angle is $\Theta \leq 90°$, the liquid (melt) exhibits wetting behavior. The interaction of the phases in contact (molten steel and ceramic substrate) becomes more likely as the wetting behavior increases. Judging by the drop silhouettes of the tested steels, it can be concluded that the interaction of Mn (XT 720) steel with the tested ceramic materials is much more pronounced than that of 11 523 steel.
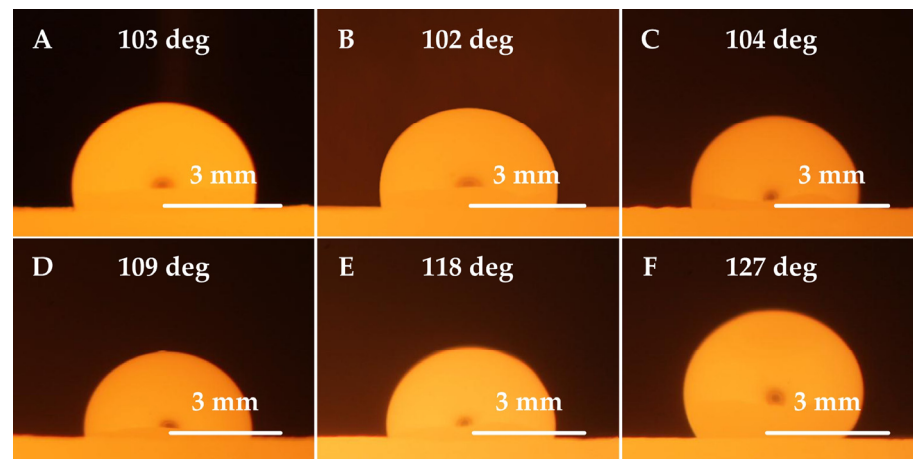
Figure 5. Images of 11 523 steel droplets wetting refractory ceramic substrates at 1550 °C; (**A**) F 36 ceramics, (**B**) ZR 50 ceramics, (**C**) B 70 ceramics, (**D**) ML 65 ceramics, (**E**) M 70 ceramics, and (**F**) MK 82 ceramics.

3.2. Degradation Testing

Figure 6 shows the degradation test results, i.e., losses of ceramics caused by high-manganese steel and low-alloy structural steel.
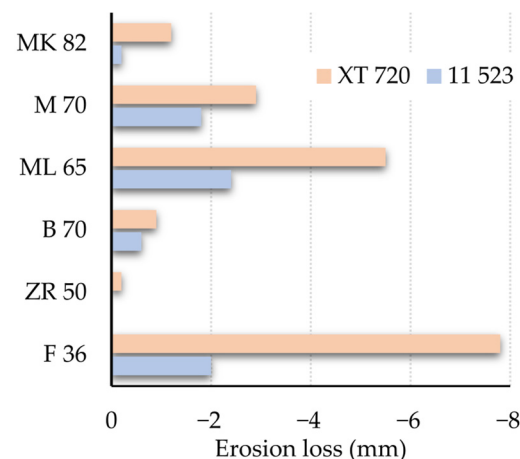

Figure 6. Degradation testing of high-manganese steel and low-alloy structural steel interactions with ceramics.

The type of steel used was found to greatly influence the degradation results of the refractories. Compared to conventional low-alloy structural steel, high-alloy manganese steel caused more significant wear to the materials tested. For this corrosive steel, the use of conventional fireclay materials proved to be entirely unsuitable. The most pronounced erosion loss interacting with this steel was observed for material F36, where even the crucible melted during the degradation tests (see Figure 7A). A more detailed discussion of the interaction is given in Section 3.3. The interaction rate of the steels with the refractory material decreases with increasing corundum content and decreasing silica and cristobalite content in the ceramics. The final state of the crucibles made from materials F36 and MK82 after degradation tests in interaction with XT 720 and 11 523 steels is shown in Figures 7A,B and 8A,B.
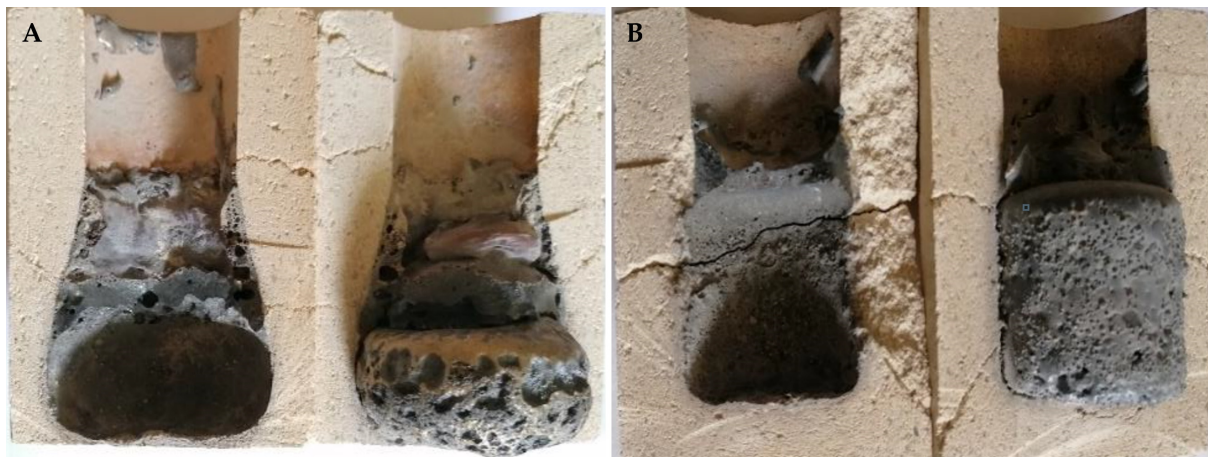
Figure 7. Degradation of refractory material F 36 after high-temperature testing; (**A**) steel XT 720, (**B**) steel 11 523.

Figure 8. Degradation of refractory material MK 82 after high-temperature testing; (**A**) steel XT 720, (**B**) steel 11 523.

3.3. Results of SEM, EDX, and XRD Analyses

After the high-temperature wetting tests, the phase interfaces between the tested steels and the corresponding refractories were subjected to SEM, EDX, and XRD analyses. It was confirmed that the high-manganese XT 720 steel interacts more strongly with the tested refractories. The results of XRD analyses for the interfacial interfaces of this steel with the conventional chamotte material F 36, the material ZR 50 containing zirconia, and the material MK 82 with the highest corundum content, are compared below and in Figure 9. The XRD analyses confirmed the formation of new phases at the interfaces. In particular, galaxite-spinel and sillimanite phases were newly identified at the interface of the F 36 material. In the case of the ZR 50 material, galaxite-spinel ($MnAl_2O_4$) and tazheranite ((Zr, Ti, Ca)O_2) phases were newly formed. Finally, for the MK 82 material, galaxite-spinel, sillimanite ($Al_2(SiO_4)O$), and tephroite (Mn_2SiO_4) phases were determined. It is worth noting that there is a high degree of isomorphic substitution in the case of spinels but in our case, it is not easy to deduce the degree of isomorphism [32]. However, qualitative evaluation points to the formation of galaxite but the formation of (Mn, Fe, Mg) (Al, Fe, Cr)$_2O_4$ ferrites cannot be excluded. The crystalline fractions for the refractory material F 36, Zr 50, and MK 82 were 31.9 wt%, 43.2 wt%, and 73.9 wt%, respectively. Thus, sample F 36 contained the most amorphous phase.
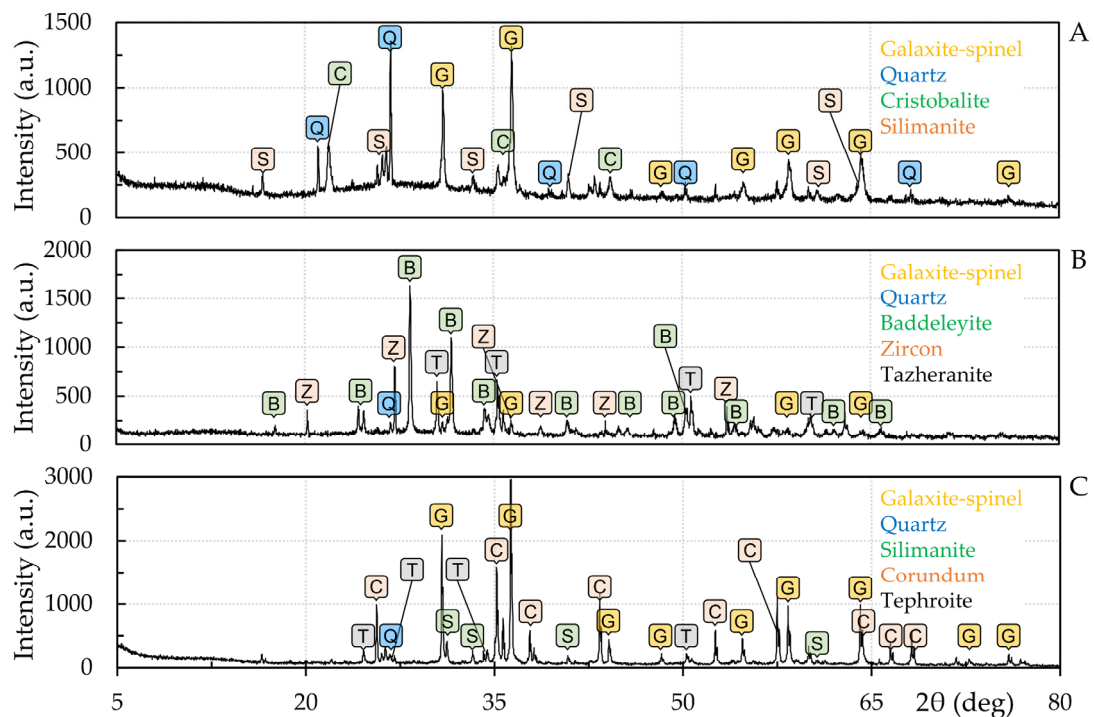
Figure 9. Diffractograms of refractory materials after high-temperature tests; (**A**) F 36 ceramics, (**B**) ZR 50 ceramics, and (**C**) MK 82 ceramics.

Based on SEM/EDX analyses (Figure 10), it can be argued that, in the case of the refractory material F 36, the main newly formed phase is the glassy phase with manganese oxide particles on its surface. Pores were also present to a higher degree in this sample, which was probably due to bubbles trapped in the rapidly cooling layer. In the case of ZR 50 ceramics, the glassy phase has also formed, and additionally, particles of baddeleyite (ZrO_2) and iron, manganese, and chromium oxide particles were identified. Ceramics MK 82 contained the least glassy phase after the high-temperature test. The crystalline phase was dominated by corundum, the crystals of which had aluminum partially substituted by manganese on their surface. In addition, aluminosilicates with manganese admixture were present, forming a dendritic structure. This structure was directed towards the hotter surface region where the crystal nucleation rate is lower in contrast to the low-temperature region where they originate. Some dendrites showed a tip-split of the primary dendritic arm, and, in addition, tertiary arm formation was observed [33]. The corresponding results of the EDX point analysis are summarized in Table 5.

Table 5. Results of semi-quantitative EDX microanalyses on the interaction of refractory samples with XT 720 steel.

Point	Caption	Mn	Si	Al	O	C	P (wt%)	Fe	Zr	Zn	Cr
1	Aluminosilicate with Mn oxide particles	36.1	20.0	10.1	33.8	—	—	—	—	—	—
2	Manganese oxide	54.8	9.5	7.4	28.3	—	—	—	—	—	—
3	Zirconium silicate	—	13.4	—	48.3	—	—	—	38.3	—	—
4	Probably Schreibersite and Fe, Mn. and Cr oxide particles	21.9	2.7	1.0	30.7	5.1	2.7	27.5	—	1.9	6.5
5	Baddeleyite	1.9	—	—	31.3	—	—	—	66.8	—	—
6	Aluminosilicate	23.9	21.5	12.8	41.8	—	—	—	—	—	—
7	Corundum (Al partially substituted by Mn)	26.2	1.3	32.1	40.4	—	—	—	—	—	—
8	Aluminosilicate with Mn oxide	42.5	18.9	8.3	30.3	—	—	—	—	—	—

In the EDX point analysis, the influence of the surroundings must be considered for small particles and thin layers.
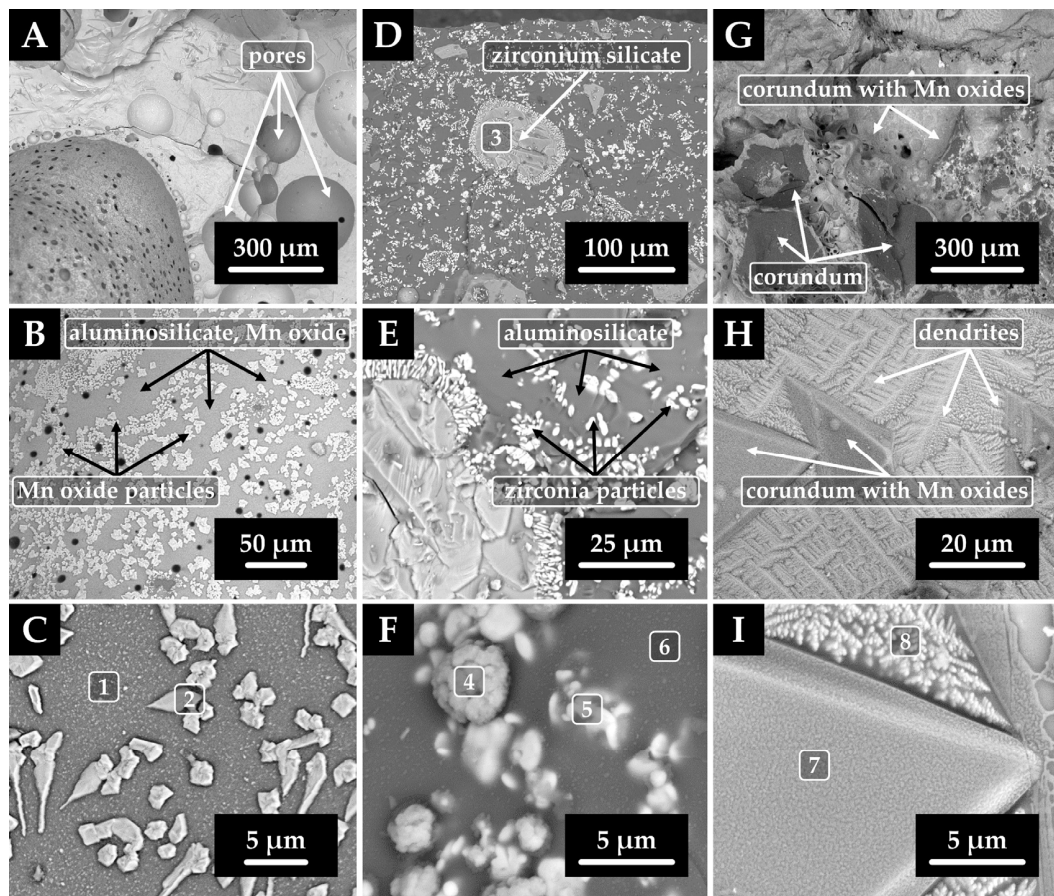
Figure 10. SEM images of refractory F 36 (**A–C**), refractory ZR 50 (**D–F**), and refractory MK 82 (**G–I**) after high-temperature test with steel XT 720; numbers 1–8 refer to EDX point analyses.

4. Conclusions

The interaction at the interface of high-manganese steel, or low-alloy construction steel, and refractory ceramics was characterized by wetting tests performed up to 1600 °C. The findings were supported by degradation tests and SEM, EDX, and XRD analyses. The findings can be summarized as:

- The intensity of the interaction at a given interface is influenced by the type of steel involved. High-manganese steel causes much more wear on refractory materials than conventional construction steel.
- Apparent wetting angles (contact angles) were significantly lower for the XT 720 steel than for the 11 523 steel. For high-manganese steel, the contact angles ranged from 10° to 103° depending on the substrate, in contrast to structural steel where non-wetting behavior was observed, and contact angles ranged from 103° to 127°. The decrease in contact angles correlated with the fraction of corundum in the refractories tested, i.e., they decreased with decreasing corundum. In addition, the contact angles decreased slightly with increasing temperature.
- The degradation tests confirmed the aggressive behavior of the XT 720 steel. The most significant erosion occurred in the case of the conventional chamotte material F 36 with a low corundum content and a higher SiO_2 and cristobalite content. Conversely, almost no erosion was observed for steel 11 523 in contact with the zirconia material ZR 50 or the high corundum material MK 82.
- The results of SEM, EDX, and XRD analyses confirmed the presence of newly formed phases at the interface of XT 720 steel with the tested refractories. In the case of the refractory material F 36, where the most significant interaction was observed, a

glassy phase with manganese-oxide particles was formed at the interface with the high manganese steel. Of the newly detected phases, galaxite-spinel and sillimanite phases were identified.

The results of this study suggest that, as the corundum content of the refractories increases, their resistance to erosion by molten steel also increases. Materials containing a higher content of fluxes (chamotte, bauxite, sintered mullite) have an increased content of the amorphous phase and show a weaker resistance to erosion. For high-alloy steels such as XT 720 steel, the use of conventional chamotte products is entirely inappropriate. For this steel, materials made of electrofused corundum can be recommended.

Author Contributions: Conceptualization, L.Ř. and V.N.; methodology, L.Ř., V.N. and S.R.; software, L.Ř., V.N. and S.R.; formal analysis, L.Ř., V.N. and S.R.; investigation, L.Ř., V.N. and D.M.; resources, L.Ř.; writing—original draft preparation, L.Ř. and V.N.; writing—review and editing, L.Ř., V.N. and S.R.; visualization, L.Ř. and V.N.; supervision, L.Ř.; project administration, S.R.; funding acquisition, L.Ř. All authors have read and agreed to the published version of the manuscript.

Institutional Review Board Statement: Not applicable.

Informed Consent Statement: Not applicable.

Data Availability Statement: The data presented in this study are available on request from the corresponding author.

Conflicts of Interest: The authors declare no conflict of interest.

Abbreviations

ADSA	Axisymmetric Drop Shape Analysis
EDX	Energy Dispersive X-ray Spectroscopy
GDOES	Glow Discharge Optical Emission Spectrometry
SEM	Scanning Electron Microscopy
XRD	X-Ray Powder Diffraction

References

1. Grässel, O.; Krüger, L.; Frommeyer, G.; Meyer, L.W. High strength Fe-Mn-(Al, Si) TRIP/TWIP steels development-properties-application. *Int. J. Plast.* **2000**, *16*, 1391–1409. [CrossRef]
2. Krawczyk, J.; Bembenek, M.; Pawlik, J. The role of chemical composition of high-manganese cast steels on wear of excavating chain in railway shoulder bed ballast cleaning machine. *Materials* **2021**, *14*, 7794. [CrossRef] [PubMed]
3. Dana, K.; Sinhamahapatra, S.; Tripathi, H.S.; Ghosh, A. Refractories of alumina-silica system. *Trans. Indian Ceram. Soc.* **2014**, *73*, 1–13. [CrossRef]
4. Fu, L.; Gu, H.; Huang, A.; Or, S.W.; Zou, Y.; Zou, Y.; Zhang, M. Design, fabrication and properties of lightweight wear lining refractories: A review. *J. Eur. Ceram. Soc.* **2022**, *42*, 744–763. [CrossRef]
5. Horckmans, L.; Nielsen, P.; Dierckx, P.; Ducastel, A. Recycling of refractory bricks used in basic steelmaking: A review. *Resour. Conserv. Recycl.* **2019**, *140*, 297–304. [CrossRef]
6. Poirier, J. A review: Influence of refractories on steel quality. *Metall. Res. Technol.* **2015**, *112*, 410. [CrossRef]
7. Wei, X.; Dudczig, S.; Storti, E.; Ilatovskaia, M.; Endo, R.; Aneziris, C.G.; Volkova, O. Interaction of molten Armco iron with various ceramic substrates at 1600 °C. *J. Eur. Ceram. Soc.* **2022**, *42*, 2535–2544. [CrossRef]
8. Wang, Y.; Huang, A.; Wu, M.; Gu, H. Corrosion of alumina-magnesia castable by high manganese steel with respect to steel cleanness. *Ceram. Int.* **2019**, *45*, 9884–9890. [CrossRef]
9. Ren, X.-M.; Ma, B.-Y.; Li, S.-M.; Li, H.-X.; Liu, G.-Q.; Yang, W.-G.; Qian, F.; Zhao, S.-X.; Yu, J.-K. Comparison study of slag corrosion resistance of MgO–$MgAl_2O_4$, MgO–CaO and MgO–C refractories under electromagnetic field. *J. Iron Steel Res. Int.* **2021**, *28*, 38–45. [CrossRef]

10. Alhussein, A.; Yang, W. Mechanism of interface reactions between Fe-2%Al alloy and high-silica tundish refractory. *Trans. Indian Inst. Met.* **2019**, *72*, 591–602. [CrossRef]
11. Alhussein, A.; Yang, W.; Zhang, L. Effect of interactions between Fe–Al alloy and MgO-based refractory on the generation of MgO·Al$_2$O$_3$ spinel. *Ironmak. Steelmak.* **2020**, *47*, 424–431. [CrossRef]
12. Jiang, M.; Wang, X.; Chen, B.; Wang, W. Formation of MgO·Al$_2$O$_3$ inclusions in high strength alloyed structural steel refined by CaO-SiO$_2$-Al$_2$O$_3$-MgO slag. *ISIJ Int.* **2008**, *48*, 885–890. [CrossRef]
13. Ehara, Y.; Yokoyama, S.; Kawakami, M. Formation mechanism of inclusions containing MgO·Al$_2$O$_3$ spinel in type 304 stainless steel. *Tetsu Hagane* **2007**, *93*, 208–214. [CrossRef]
14. Park, J.H.; Lee, S.-B.; Gaye, H.R. Thermodynamics of the formation of MgO-Al$_2$O$_3$-TiO$_x$ inclusions in Ti-stabilized 11Cr ferritic stainless steel. *Metall. Mater. Trans. B* **2008**, *39*, 853–861. [CrossRef]
15. Zhang, L.; Thomas, B.G. State of the art in the control of inclusions during steel ingot casting. *Metall. Mater. Trans. B* **2006**, *37*, 733–761. [CrossRef]
16. Park, J.H.; Zhang, L. Kinetic modeling of nonmetallic inclusions behavior in molten steel: A review. *Metall. Mater. Trans. B* **2020**, *51*, 2453–2482. [CrossRef]
17. Polkowski, W.; Sobczak, N.; Polkowska, A.; Nowak, R.; Kudyba, A.; Bruzda, G.; Giuranno, D.; Generosi, A.; Paci, B.; Trucchi, D.M. Ultra-high temperature interaction between h-BN-based composite and molten silicon. *Metall. Mater. Trans. A* **2019**, *50*, 997–1008. [CrossRef]
18. López, V.H.; Kennedy, A.R. Flux-assisted wetting and spreading of Al on TiC. *J. Colloid Interface Sci.* **2006**, *298*, 356–362. [CrossRef]
19. Kumar, G.; Prabhu, K.N. Review of non-reactive and reactive wetting of liquids on surfaces. *Adv. Colloid Interface* **2007**, *133*, 61–89. [CrossRef]
20. Shibata, H.; Jiang, X.; Valdez, M.; Cramb, A.W. The contact angle between liquid iron and a single-crystal magnesium oxide substrate at 1873 K. *Metall. Mater. Trans. B* **2004**, *35*, 179–181. [CrossRef]
21. Eustathopoulos, N.; Voytovych, R. The role of reactivity in wetting by liquid metals: A review. *J. Mater. Sci.* **2016**, *51*, 425–437. [CrossRef]
22. Sobczak, N.; Singh, M.; Asthana, R. High-temperature wettability measurements in metal/ceramic systems—Some methodological issues. *Curr. Opin. Solid State Mater. Sci.* **2005**, *9*, 241–253. [CrossRef]
23. Zhou, X.B.; De Hosson, J.T.M. Reactive wetting of liquid metals on ceramic substrates. *Acta Mater.* **1996**, *44*, 421–426. [CrossRef]
24. Wang, L.; Zhu, H.; Zhao, J.; Song, M.; Xue, Z. Steel/refractory/slag interfacial reaction and its effect on inclusions in high-Mn high-Al steel. *Ceram. Int.* **2022**, *48*, 1090–1097. [CrossRef]
25. Alibeigi, S.; Kavitha, R.; Meguerian, R.J.; McDermid, J.R. Reactive wetting of high Mn steels during continuous hot-dip galvanizing. *Acta Mater.* **2011**, *59*, 3537–3549. [CrossRef]
26. Pourmajidian, M.; McDermid, J.R. On the reactive wetting of a medium-Mn advanced high-strength steel during continuous galvanizing. *Surf. Coat. Technol.* **2019**, *357*, 418–426. [CrossRef]
27. Yang, T.; He, Y.; Chen, Z.; Zheng, W.; Wang, H.; Li, L. Effect of dew point and alloy composition on reactive wetting of hot dip galvanized medium manganese lightweight steel. *Coatings* **2020**, *10*, 37. [CrossRef]
28. Kong, L.; Deng, Z.; Zhu, M. Reaction behaviors of Al-killed medium-manganese steel with different refractories. *Metall. Mater. Trans. B* **2018**, *49*, 1444–1452. [CrossRef]
29. Saad, S.M.I.; Neumann, A.W. Axisymmetric drop shape analysis (ADSA): An outline. *Adv. Colloid. Interface* **2016**, *238*, 62–87. [CrossRef]
30. Brooks, R.F.; Quested, P.N. The surface tension of steels. *J. Mater. Sci.* **2005**, *40*, 2233–2238. [CrossRef]
31. Dubberstein, T.; Heller, H.-P.; Klostermann, J.; Schwarze, R.; Brillo, J. Surface tension and density data for Fe–Cr–Mo, Fe–Cr–Ni, and Fe–Cr–Mn–Ni steels. *J. Mater. Sci.* **2015**, *50*, 7227–7237. [CrossRef]
32. Lu, Z.; Wang, Z.; Wang, S.; Zhao, H.; Cai, Z.; Wang, Y.; Ma, H.-A.; Chen, L.; Jia, X. Orientational dependences of diamonds grown in the NiMnCo-Silicate-H$_2$O-C system under HPHT conditions and implications to natural diamonds. *ACS Earth Space Chem.* **2022**, *6*, 987–998. [CrossRef]
33. Bhagurkar, A.G.; Qin, R. The microstructure formation in slag solidification at continuous casting mold. *Metals* **2022**, *12*, 617. [CrossRef]